Chinese Chemical Letters 36 (2025) 110106

Contents lists available at ScienceDirect

Chinese Chemical Letters

journal homepage: www.elsevier.com/locate/cclet

Differential releasing hydrogel loaded with oncolytic viruses and anti-CAFs drug to enhance oncology therapeutic efficacy

Xiaoyu Hou[a,b,c,1], Mingyang Liu[a,b,c,1], Hu Wu[a,b,c,1], Nan Wang[a,c,1], Xu Zhao[a,b,c], Xifeng Qin[b], Xiaomin Su[d], Hanwei Huang[a,b,c], Zihan Ma[a,c], Jiahao Liu[a,c], Onder Ergonul[e], Füsun Can[e], Wei Liu[f,*], Zhiqing Pang[b,*], Funan Liu[a,c,g,*]

[a] Department of Surgical Oncology and General Surgery, The First Hospital of China Medical University, Shenyang 110001, China
[b] Department of Pharmaceutics, School of Pharmacy, Fudan University and Key Laboratory of Smart Drug Delivery, Ministry of Education, Shanghai 201203, China
[c] Key Laboratory of Precision Diagnosis and Treatment of Gastrointestinal Tumors, China Medical University, Ministry of Education, Shenyang 110001, China
[d] Central Laboratory, First Affiliated Hospital, Institute (College) of Integrative Medicine, Dalian Medical University, Dalian 116021, China
[e] Koç University Iş Bank Center for Infectious Diseases (KUISCID), Koç University School of Medicine and American Hospital, Istanbul 34450, Turkey
[f] The First Affiliated Hospital of Jinzhou Medical University, Jinzhou 121001, China
[g] Phase I Clinical Trials Center, The First Hospital, China Medical University, Shenyang 110102, China

ARTICLE INFO

Article history:
Received 7 April 2024
Revised 10 June 2024
Accepted 11 June 2024
Available online 18 June 2024

Keywords:
Cancer-associated fibroblasts
Oncolytic virus
Hydrogel
Differential release
Immunology

ABSTRACT

Interstitial hypertension and extracellular matrix (ECM) barriers imposed by cancer-associated fibroblasts (CAFs) at the tumor site significantly impede the retention of intratumorally administered oncolytic viruses (OVs) as well as their efficacy in infecting and eradicating tumor cells. Herein, a stable, controllable, and easily prepared hydrogel was developed for employing a differential release strategy to deliver OVs. The oncolytic herpes simplex virus-2 (oH2) particles were loaded within sodium alginate (ALG), together with the small molecule drug PT-100 targeting CAFs. The rapid release of PT-100 functions as an anti-CAFs agent, reducing ECM, and alleviating interstitial pressure at the tumor site. Consequently, the delayed release of oH2 could more effectively invade and eradicate tumor cells while also facilitating enhanced infiltration of immune cells into the tumor microenvironment, thereby establishing an immunologically favorable milieu against tumors. This approach holds significant potential for achieving highly efficient oncolytic virus therapy with minimal toxicity, particularly in tumors rich in stromal components.

Oncolytic viruses (OVs) are a promising emerging class of anticancer immunotherapies that exploit the innate ability of certain replication-competent viruses to infect and preferentially lyse tumor cells while leaving non-neoplastic cells intact [1,2]. In recent years, OVs immunotherapy has thrived in the field of tumor treatment, with numerous clinical and basic studies being continuously reported [3–8]. A growing body of evidence suggests that the cytotoxic effect of OVs on tumor cells is not solely attributed to direct lysis, but rather involves a complex regulatory mechanism that integrates multiple pathways [9,10]. The mechanisms encompass the modulation of alterations in both the tumor microenvironment (TME) and macroenvironment, as well as $CD8^+$ T cell-mediated specific immune responses and innate immune cellular responses [11–13].

The current clinical use of OVs products is limited to four approved options, all of which are exclusively administered *via* intratumoral injection [14]. Intratumoral administration allows precise control of OVs concentrations in the TME, resulting in better therapeutic outcomes [1,14]. However, the intricate TME, characterized by an abundance of extracellular matrix (ECM) and elevated interstitial pressure at the tumor site, poses a challenge for intratumoral administration of OVs as it may result in nonspecific shedding into adjacent healthy tissues, thereby potentially leading to adverse reactions, such as mild hepatotoxicity, as reported in some studies [15]. Moreover, physical barriers also pose significant challenges for the penetration and spread of OVs. The cancer-associated fibroblasts (CAFs), which actively promotes tumor maintenance through interactions with tumor cells and cellular components in the TME, acts as a major barrier to the dissemination of OVs [16]. Therefore,

* Corresponding authors.
E-mail addresses: 39240031@qq.com (W. Liu), zqpang@fudan.edu.cn (Z. Pang), fnliu@cmu.edu.cn (F. Liu).
[1] These authors contributed equally to this work.

https://doi.org/10.1016/j.cclet.2024.110106
1001-8417/

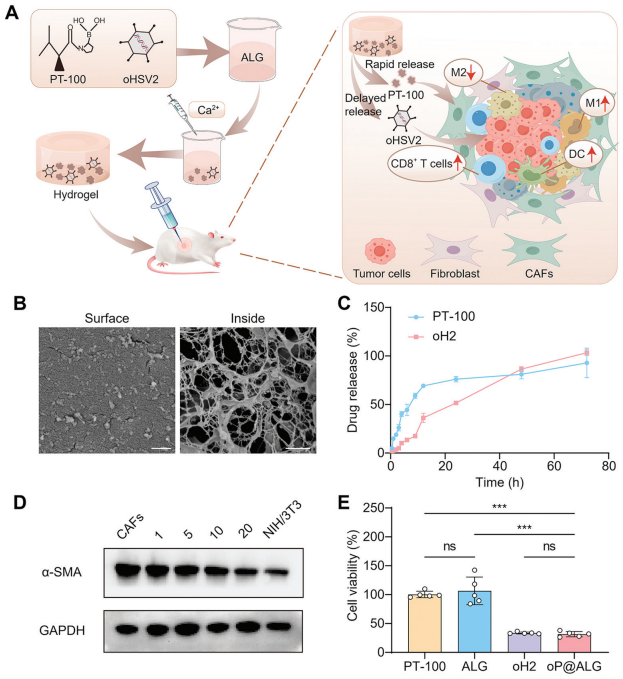

Fig. 1. Preparation and characterization of oP@ALG. (A) Schematic illustration of the preparation process of oP@ALG and the mechanism of oP@ALG after intratumoral injection. (B) Representative cryo-SEM images of oP@ALG. Scale bar: 400 nm (left) and 1 μm (right). (C) Release curves of oH2 and PT-100, $n = 3$. (D) The expression of α-SMA in CAFs treated with different concentrations of PT-100 for 48 h, the group of CAFs without PT-100-treated as the positive group and the NIH/3T3 cells without PT-100-treated as the control group. (E) Cell viability of CT26 cells after treatment with PT-100/ALG/oH2/oP@ALG for 48 h, $n = 5$. Data are displayed as mean ± SD. The data in (C) are presented as the percentage of the total dose. The data in (E) are presented as a relative percentage compared to the normal CT26 cells. Statistical significance was analyzed by one-way ANOVA with a Tukey *post hoc* test; ns, no significant difference. $^{***}P < 0.001$.

modulation of CAFs becomes essential for augmenting the efficacy of OVs.

Herein, to achieve efficient retention of intratumorally injected oncolytic herpes simplex virus-2 (oH2), enhance tumor cell infection and trigger antitumor immunity, a differential drug-release hydrogel was developed. As shown in Fig. 1A, sodium alginate (ALG), oH2 particles, and PT-100 were thoroughly mixed *in vitro* and then injected intratumorally into the tumor site to form a hydrogel through cross-linking of ALG with Ca^{2+} at physiological concentration. The resulting hydrogel (oP@ALG) encapsulates oH2 within ALG, along with the small molecule drug PT-100 targeting anti-CAFs. The inadvertent distribution of oH2 to non-target tissues was alleviated through the incorporation of hydrogel, which effectively prevented potential toxicity. Additionally, the fast-releasing PT-100 acts as an anti-CAFs drug that normalizes CAFs while reducing ECM content and interstitial pressure at the tumor site. And the slow-releasing oH2 effectively infects and kills tumor cells. The differential release strategy employed by this hydrogel synergistically promotes immune cell infiltration and cytotoxicity leading to increased infiltration of $CD8^+$ T cells, dendritic cells (DCs), and M1 macrophages at the tumor site while decreasing M2 macrophages. This creates an anti-tumor immune microenvironment that enhances OVs efficacy. Overall, our approach provides a promising paradigm for highly effective yet low-toxicity OVs therapy particularly suitable for stroma-rich tumors.

The oP@ALG was obtained by thoroughly mixing ALG with oH2 and PT-100. Similarly, the oH@ALG was conducted by thoroughly mixing ALG with oH2 and the PT@ALG was prepared by thoroughly mixing ALG with PT-100. The formation of hydrogel *in vitro* was first confirmed. The oH2-Cy5.5@ALG solution rapidly formed a hydrogel upon extrusion from the needle tip into the surrounding fluids with intratumoral calcium concentration, exhibiting no morphological changes within 3 h (Figs. S1A and S2 in Supporting information). On the contrary, free oH2-Cy5.5 dispersed quickly throughout the beaker when injected into the Ca^{2+}-containing solution. This result suggests that the cross-linking of ALG with Ca^{2+} shows an effective ability to immobilize the drug in the hydrogel. In addition, we explored the effect of different concentrations of ALG on the formation of hydrogels from oP@ALG. As shown in Fig. S1B (Supporting information), hydrogel formation depended on the concentration of ALG. When the concentration of ALG was only 1 or 2 mg/mL, the mixture diffused rapidly at the bottom of the cup due to its weak gelation. When the ALG concentration was raised to 5, 10, and 20 mg/mL, the oH2-Cy5.5@ALG quickly turned into the hydrogels in the Ca^{2+} solution. It is worth noting that when the concentration of ALG was >5 mg/mL, the viscosity was too large and not conducive to injection. Additionally, 5 mg/mL of ALG was added to the Ca^{2+} solution to form a hydrogel with weaker mechanical intensity and variable morphology. Based on the above results, ALG concentration of 5 mg/mL was selected for subsequent experiments. To further investigate the properties of the hydrogels, rheometers were employed to examine the rheology and viscosity of hydrogels. In rheological analysis experiments, when the elastic modulus (G') is greater than the viscosity modulus (G"), the sample is defined as a solid rather than a liquid [17,18]. As shown in Fig. S3A (Supporting information), G' was significantly larger than G", indicating that ALG could form hydrogels by chelation with Ca^{2+}. Besides, we also explored the relationship between the viscosity of the hydrogel and the shear rate. As shown in Fig. S3B (Supporting information), the viscosity of the oP@ALG hydrogel gradually decreased with the increase of the shear rate, signifying the presence of shear thinning behavior within the hydrogel, while the viscosity of the oP@ALG solution did not exhibit significant changes. The formation of oP@ALG hydrogel was then examined by confocal laser scanning microscopy (CLSM) and cryo-scanning electron microscope (cryo-SEM). As presented in Fig. S4 (Supporting information), the distribution of Cy5.5-labeled oH2 within the FITC-labeled ALG hydrogel was observed to be uniform. Additionally, surface aggregation of oH2 particles on the hydrogel was evident, accompanied by the formation of a cross-linked mesh structure inside the hydrogel (Fig. 1B). The differential release capability of oP@ALG was further validated by quantifying the release of each component at different time intervals. The release of PT-100 exhibited a rapid increase up to 4 h, accounting for approximately 40% of the total release (Fig. 1C and Fig. S5 in Supporting information). The release rate of oH2 was significantly reduced compared to PT-100, with only a 10% release observed over a period of 4 h. This disparity can be attributed to the larger particle size of the oH2 viral particles, which function as nanoparticles rather than free drug. The aforementioned statement is in complete alignment with the differential release strategy employed for hydrogel-loaded drugs in this study. Specifically, the rapid-release PT-100 functions as an anti-CAFs agent to normalize CAFs and alleviate mesenchymal pressure at the tumor site. Subsequently, the slow-release oH2 effectively infects and eradicates tumor cells.

The anti-CAFs efficacy of PT-100 was subsequently validated. The differentiation of mouse embryonic fibroblasts (NIH/3T3) into CAFs was firstly achieved by using transforming growth factor-β1 (TGF-β1), following a previously established protocol [19]. As presented in Fig. S6B (Supporting information), CAFs showed a 0.72-fold increase in the proliferative capacity compared with NIH/3T3. The PT-100 did not exhibit a detrimental effect on NIH/3T3 cells across a wide concentration range (Fig. S6A in Supporting information), while significantly inhibiting the proliferative capacity of CAFs (Fig. S6B). Furthermore, following treatment with PT-100,

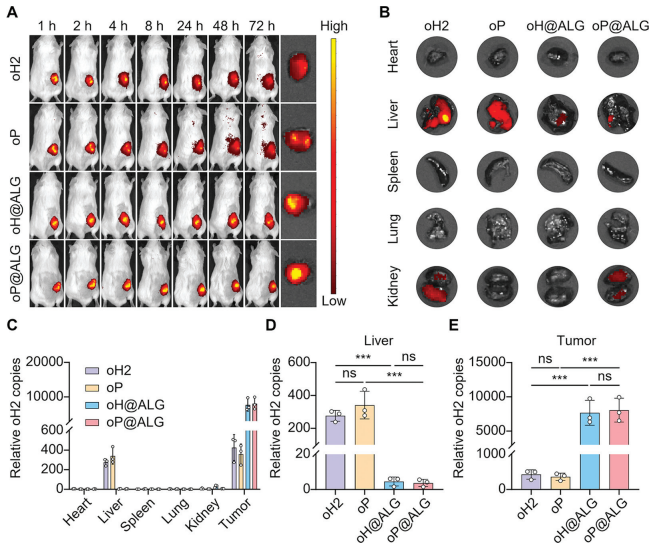

Fig. 2. oP@ALG prolonged oH2 retention and reduced oH2 escape at the tumor site. (A) *In vivo* fluorescence imaging of tumors at different time points after intratumoral injection of Cy5.5-labeled oH2, oP, oH@ALG, and oP@ALG. (B) *In vitro* fluorescence imaging of vital organs at 72 h after intratumoral injection of Cy5.5-labeled oH2, oP, oH@ALG, and oP@ALG by IVIS. (C-E) The quantitative distribution of oH2, oP, oH@ALG, and oP@ALG in vital organs, (D) livers and (E) tumors determined by qPCR assay at 48 h after intratumoral injection, $n = 3$. Data are displayed as mean ± SD. The data in (C–E) are presented as relative copies compared to the PBS group. Statistical significance was analyzed by one-way ANOVA with a Tukey *post hoc* test. $^{***}P < 0.001$.

there was a significant decrease in the expression of α-smooth muscle actin (α-SMA), a marker indicative of activated CAFs (Fig. 1D). These results suggested that PT-100, as an anti-CAFs drug, acts mainly by normalizing CAFs into normal fibroblasts. The tumor cell killing ability of different components of oP@ALG was subsequently investigated. The growth inhibition ability of ALG and PT-100 for CT26 cells was not significant (Fig. 1E and Fig. S7 in Supporting information). Conversely, the concentration-dependent killing ability of oH2 on CT26 cells exhibited an increase. These findings suggest that PT-100 in oP@ALG can normalize CAFs and oH2 in oP@ALG could kill tumor cells.

The intratumoral administration of OVs has been reported to induce mild hepatotoxicity in cancer patients, attributed to the non-specific dissemination of viral vectors into the surrounding healthy tissues [15]. To determine whether the hydrogel matrix prolongs oH2 retention at the tumor site as well as reduces oH2 shedding to non-target tissues, the biodistribution of each oH2 formulations were investigated by an *in vivo* imaging system (IVIS). All animal protocols were approved by the Animal Ethics Committee of Fudan University. As illustrated in Fig. 2A, the fluorescence intensity of Cy5.5-labeled oP@ALG and oH@ALG at the tumor site was significantly higher than that of oH2 and oP (formulations prepared by mixing oH2 with PT-100) at 8, 24, 48, or 72 h after intratumoral injection. The drug fluorescence at the tumor site in the oH2 and oP groups gradually dissipated over time due to the absence of hydrogel as a carrier. The tumors and other major organs (heart, liver, spleen, lung, and kidney) were extracted from the mice following the final imaging of mice for subsequent *in vitro* fluorescence analysis. The results indicated that the livers of mice in the oH2 and oP groups exhibited intense fluorescent signals, while weaker fluorescent signals could be observed in the oH@ALG and oP@ALG groups (Fig. 2B). The significance of the hydrogel in minimizing the distribution of free oH2 to non-target tissues was demonstrated by this result.

In order to precisely quantify the amount of oH2 in major organs, quantitative real-time polymerase chain reaction (qPCR) assay was performed. As shown in Figs. 2C–E, the oH2 distribution in the liver was reduced by more than 95% in the oH2@ALG and oP@ALG groups compared to the oH2 and oP groups, suggesting that sustained release of oH2 from the hydrogel reduces viral shedding to the liver. Meanwhile, the oH2 retention in the tumor was increased 18-fold in the oH2@ALG and oP@ALG groups relative to the oH2 and oP groups, indicating that the hydrogel matrix could significantly prolong the retention time of oH2 in the tumor site. Taken together, these results suggest that the oP@ALG hydrogel system can maintain a higher concentration of oH2 in tumor tissues and prevent viral shedding to non-target tissues at an early stage and for a longer period of time.

The anti-tumor efficacy of oP@ALG was initially examined in a murine subcutaneous tumor model (Fig. 3A). The tumor volume exhibited a rapid increase in the phosphate saline buffer (PBS) group, whereas neither oH@ALG nor PT@ALG presented significant inhibitory effects on tumor growth. Encouragingly, oP@ALG demonstrated complete inhibition of tumor growth, potentially attributed to the remodeling effect of PT-100 and oH2 on the TME and the immobilization ability of hydrogel (Figs. 3B–D). The rapid release of PT-100 from the hydrogel that normalized CAFs enhanced the infectious and killing effects of oH2 on tumor cells and promoted immune cell infiltration, thus enhancing the effects of OVs therapy and immunotherapy. Tumor weights in the oP@ALG group were only 26.47%, 29.38%, and 27.27% of that in the PBS, oH@ALG, and PT@ALG groups, respectively (Fig. 3C). The tumor slices exhibited a significant cellular gap in the group with the presence of PT-100, indicating a significant reduction in the ECM secreted by CAFs after PT-100 treatment (Fig. 3E). Immunofluorescence sections also showed a significant decrease in the fluorescence intensity and proportion of α-SMA in the tumors treated with PT-100, indicating a decrease in the amount of CAFs compared to the PBS group and the oH@ALG group (Fig. 3F). Additionally, comparable body weights among all groups and the histological examination of major organs confirmed the safety profile of oP@ALG treatment (Figs. S8 and S9 in Supporting information). All the results unequivocally demonstrate that oP@ALG displays remarkable antitumor efficacy.

Abundant infiltration of $CD8^+$ T cells in the tumors could be observed in the tumors after oP@ALG treatment, while the remaining three groups had only a small amount of T cell infiltration (Figs. S10 and S11 in Supporting information). Moreover, a higher expression of tumor necrosis factor-α (TNF-α) was observed in the tumors of the oP@ALG group compared to other groups, thereby promoting an enhanced anti-tumor immune response (Fig. S12 in Supporting information). The flow cytometry assay was then performed to accurately assess the immune response in tumor tissue. As shown in Fig. 4A and Fig. S13 (Supporting information), the amount of $CD8^+$ T cells in the tumors of the oP@ALG group was 2.28, 2.16, and 2.38 times higher than that in the PBS, oH@ALG, and PT@ALG groups, respectively. Furthermore, the amount of $CD80^+CD86^+$ cells in the tumors of the oP@ALG group was 1.81, 1.34, and 1.55 times higher than that in the PBS, oH@ALG, and PT@ALG groups, respectively (Fig. 4B and Fig. S14 in Supporting information). Notably, the number of anti-tumor M1 macrophages in tumors treated with oP@ALG was at least twice as high as in the other groups (Fig. 4C and Fig. S15 in Supporting information). In contrast, the proportion of M2 macrophages in the oP@ALG group decreased 3.17-fold and 2.15-fold compared to the PBS and oH@ALG groups, respectively (Fig. 4D). Taken together, these results suggested that oP@ALG could promote the tumor immune microenvironment.

Encouraged by the potent effects of oP@ALG in regulating stroma and inhibiting tumor growth (Fig. 3), a stroma-rich subcutaneous tumor model was established to further investigate the anti-tumor efficacy of oP@ALG, and the treatment schedule was

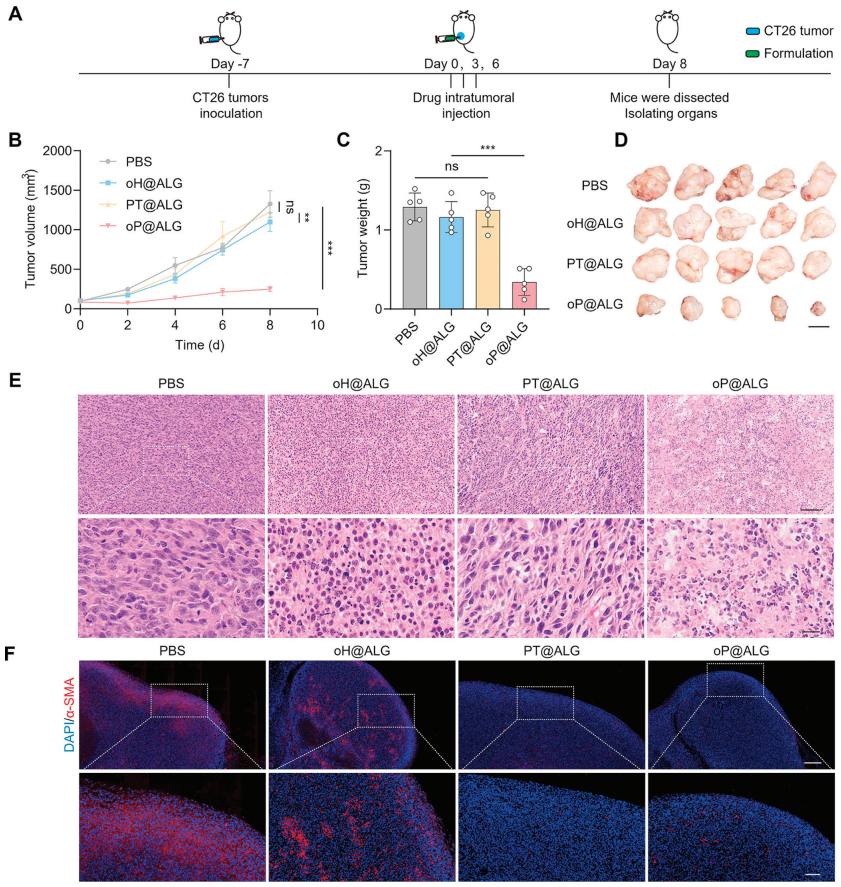

Fig. 3. *In vivo* therapeutic efficacy of oP@ALG against CT26 subcutaneous tumor model. (A) Schematic illustration of dosing regimens of oH@ALG, PT@ALG and oP@ALG in CT26 subcutaneous tumor models. (B) The tumor growth profiles, (C) the tumor weight, and (D) tumor photos after various treatments. $n = 5$. Scale bar: 10 mm. (E) H&E staining of tumor tissue sections after various treatments at day 8. Scale bar: 100 μm (at low magnification), 20 μm (at high magnification). (F) Immunofluorescence staining of α-SMA of tumor tissue sections after various treatments at day 8. Scale bar: 400 μm (at low magnification), 100 μm (at high magnification). Data are displayed as mean ± SD. Statistical significance was analyzed by one-way ANOVA with a Tukey *post hoc* test. $^{**}P < 0.01$, $^{***}P < 0.001$.

presented in Fig. 5A. Tumor growth was significantly inhibited after oP@ALG treatment, while other treatments had little impact on tumor progression (Figs. 5B–D). There were no significant differences in the body weight of mice in all groups during the treatment, indicating the safety of oP@ALG treatment (Fig. S16 in Supporting information). Consistent with the results in the CT26 subcutaneous tumor model (Fig. 3), PT-100 treatment resulted in the normalization of CAFs and reduction in ECM, ultimately enhancing the anti-tumor efficacy of oH2 (Figs. 5E and F). In addition, more $CD8^+$ T cells and higher expressions of interleukin 6 (IL-6), TNF-α, and interferon gamma (IFN-γ) could be observed in tumors of the oP@ALG group compared with other groups (Figs. S17–S19 in Supporting information). And the major organs of the oP@ALG group exhibited minimal cytotoxic effects, indicating a negligible impact on their functionality (Fig. S20 in Supporting information).

The ability of oP@ALG to prevent tumor recurrence was evaluated through a post-tumor resection model and the treatment regimen was illustrated in Fig. 5G. The growth of tumors in mice treated with oH@ALG or PT@ALG exhibited a slight delay, however, tumor recurrence still occurred (Fig. 5H). The mice treated with oP@ALG exhibited a pronounced inhibition of tumor recurrence, with no tumors detected in 5 out of 8 mice within this experimental group (Figs. 5I and J). These findings strongly suggest that oP@ALG possesses a significant advantage in effectively suppressing tumor recurrence following surgical intervention. Similarly, there was no significant difference in body weight of the mice in other groups throughout the experimental period, except that the PT@ALG-treated mice lost body weight, which could be attributed to the differences in the rate of recovery after surgery among the different mice (Fig. S21 in Supporting information). These results demonstrate that the oP@ALG hydrogel system shows excellent therapeutic efficacy not only in the CT26 subcutaneous tumor model, but also in close-to-clinical tumor models, such as the stroma-rich subcutaneous tumor model and the post-tumor resection model, which show a strong ability to inhibit tumor growth.

Herpes simplex virus (HSV), which exists in two strains: HSV-1 and HSV-2, is one extensively studied virus for OV therapy. The genetically engineered Talimogene Laherparepvec (T-VEC) is a representative oncolytic herpes simplex virus type 1 (oHSV1) [20]. T-VEC therapy has been successfully evaluated for safety and efficacy in several different cancer types [21–24]. Additionally, a recent clinical study demonstrated that oH2, constructed based on HSV-2, exhibited favorable safety profiles along with encouraging anti-tumor activity in patients with metastatic rectal and esophageal cancer [25]. In this study, a stable, controllable, and easily prepared hydrogel was developed for employing a differential release strategy to deliver OVs. The oH2 particles were loaded within ALG, together with the small molecule drug PT-100 targeting CAFs. ALG consists of regions containing guluronic and mannuronic acid, which could rapidly bind with Ca^{2+} *in vivo*, forming an "egg box" structure. One of the key characteristics of ALG is its capability to form an *in-situ* hydrogel [17,26–29]. Being biocompatible and biodegradable, ALG has been utilized as a drug carrier for achieving controlled release of drugs within tumor tissues. Compared to other gels, ALG exhibits excellent properties such as softness, non-toxicity, high wa-

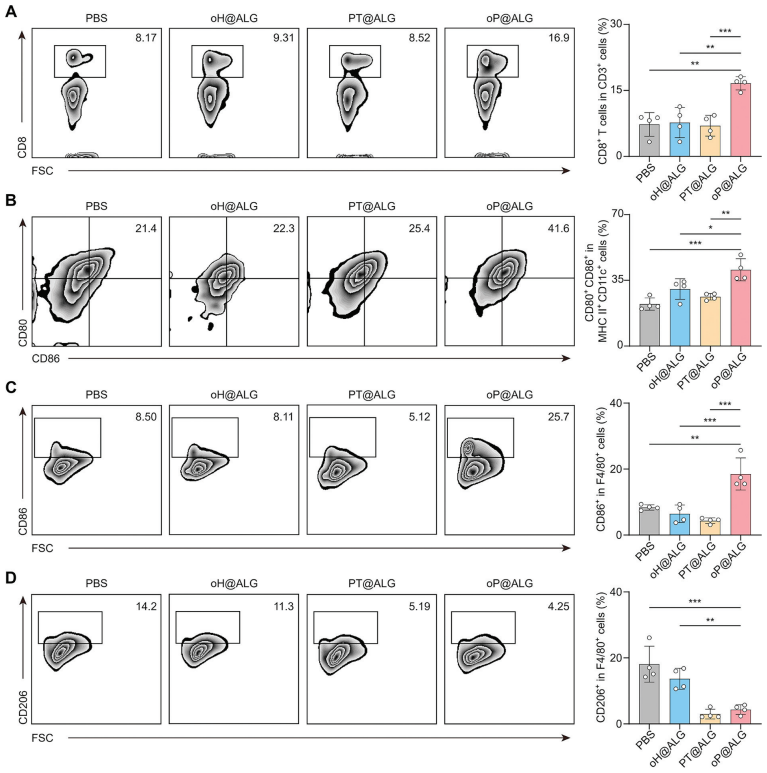

Fig. 4. oP@ALG promoted the antitumor immune response in CT26 subcutaneous tumor models. (A) Representative flow cytometry plots and the corresponding quantitative analysis of $CD8^+$ T cells gating on $CD3^+$ cells in tumors, $n = 4$. (B) Representative flow cytometry plots and the corresponding quantitative analysis of $CD80^+CD86^+$ cells gating on MHC II^+ $CD11c^+$ cells in tumors, $n = 4$. (C) Representative flow cytometry plots and the corresponding quantitative analysis of $CD86^+$ cells gating on $F4/80^+$ cells in tumors, $n = 4$. (D) Representative flow cytometry plots and the corresponding quantitative analysis of $CD206^+$ cells gating on $F4/80^+$ cells in tumors, $n = 4$. Data are displayed as mean ± SD. The animal model was CT26 subcutaneous tumors in the BALB/c mice, and the sampling time was two days after the second injection. Statistical significance was analyzed by one-way ANOVA with a Tukey *post hoc* test. $^*P < 0.05$, $^{**}P < 0.01$, $^{***}P < 0.001$.

ter content, and a structure resembling that of ECM. Consequently, it finds extensive applications as a drug carrier, cell transplantation material, and wound dressing agent [30–36]. The use of ALG-loaded OVs to form hydrogels allows OVs to maintain relatively high drug concentrations at the tumor site and prevents viral shedding to non-target tissues at an early stage and over a longer period of time, thus avoiding off-target toxicity of OVs.

Tumor stroma, with its specific biological characteristics such as tissue hypoxia and acidosis, mesenchymal hyperpressure formation, *etc*., plays a crucial role in tumorigenesis, progression, metastasis, and treatment resistance. CAFs are an integral component of the tumor stroma [37]. The secretion of various cytokines or metabolites by CAFs not only hampers immune cell function, promoting tumor development, invasion, and metastasis but also remodels the extratumoral stroma and establishes a barrier against drug penetration and therapeutic immune cells. This impediment significantly compromises the efficacy of tumor therapy [38,39]. Therefore, numerous studies have focused on modulating CAFs or overcoming their barrier effect to inhibit tumors [19,40–42]. Physical barriers also pose significant challenges for the penetration and spread of OVs. The CAFs, which actively promotes tumor maintenance through interactions with tumor cells and cellular components in the TME, acts as a major barrier to OV dissemination. Therefore, modulation of CAFs becomes essential for augmenting OV efficacy. PT-100 functions as an inhibitor for fibroblast activation protein (FAP) by suppressing transformation of fibroblasts into CAFs induced by stimulatory factors secreted by both tumor cells and normal cells; this normalization process converts CAFs back into normal fibroblasts thereby reducing secretion levels of ECM components along with immunosuppressive cytokines leading to alleviation of immunosuppressive microenvironment conditions within tumors while enhancing immune cell infiltration rates along with restoration viability levels among immune cells [40,43–45]. The rapid release of PT-100 in oP@ALG functions as an anti-CAFs agent, reducing ECM, and alleviating interstitial pressure at the tumor site. Consequently, the delayed release of oH2 could more effectively invade and eradicate tumor cells. The infection and replication of OVs in the tumor ultimately leads to cancer cell lysis, releasing large amounts of tumor antigens and inflammatory mediators, which promotes an anti-tumor immune response [2,14]. Normalization of CAF combined with anti-tumor immunity induced by oH2 could further promote the infiltration and cytotoxicity of immune cells, thus constructing an anti-tumor immune microenvironment and enhancing the therapeutic efficacy.

The *in vitro* results showed that ALG could successfully load and then differential release PT-100 and oH2, which could be attributed to the larger particle size of the oH2 viral particles, which function as nanoparticles rather than free drug. We then performed cytological experiments showed that PT-100 in oP@ALG normalized CAFs, while oH2 killed tumor cells. In CT26 subcutaneous tumor model pharmacodynamics experiments, oP@ALG showed superior anti-tumor efficacy and significantly induced an anti-tumor immune microenvironment. Similarly, oP@ALG demonstrated impressive therapeutic and immune-triggering effects in a stroma-rich subcutaneous tumor model. At present, one of the main factors affecting the recurrence and poor prognosis of clinical tumors is that the tumor cannot be completely removed during surgical resection. Therefore, after conducting a pharmacodynamic experiment of drug inhibition of tumor growth, we further investigated the effect of a single injection at the original tumor site immediately after tumor resection on postoperative residual tumor. The results showed that a single injection of oP@ALG at the surgical

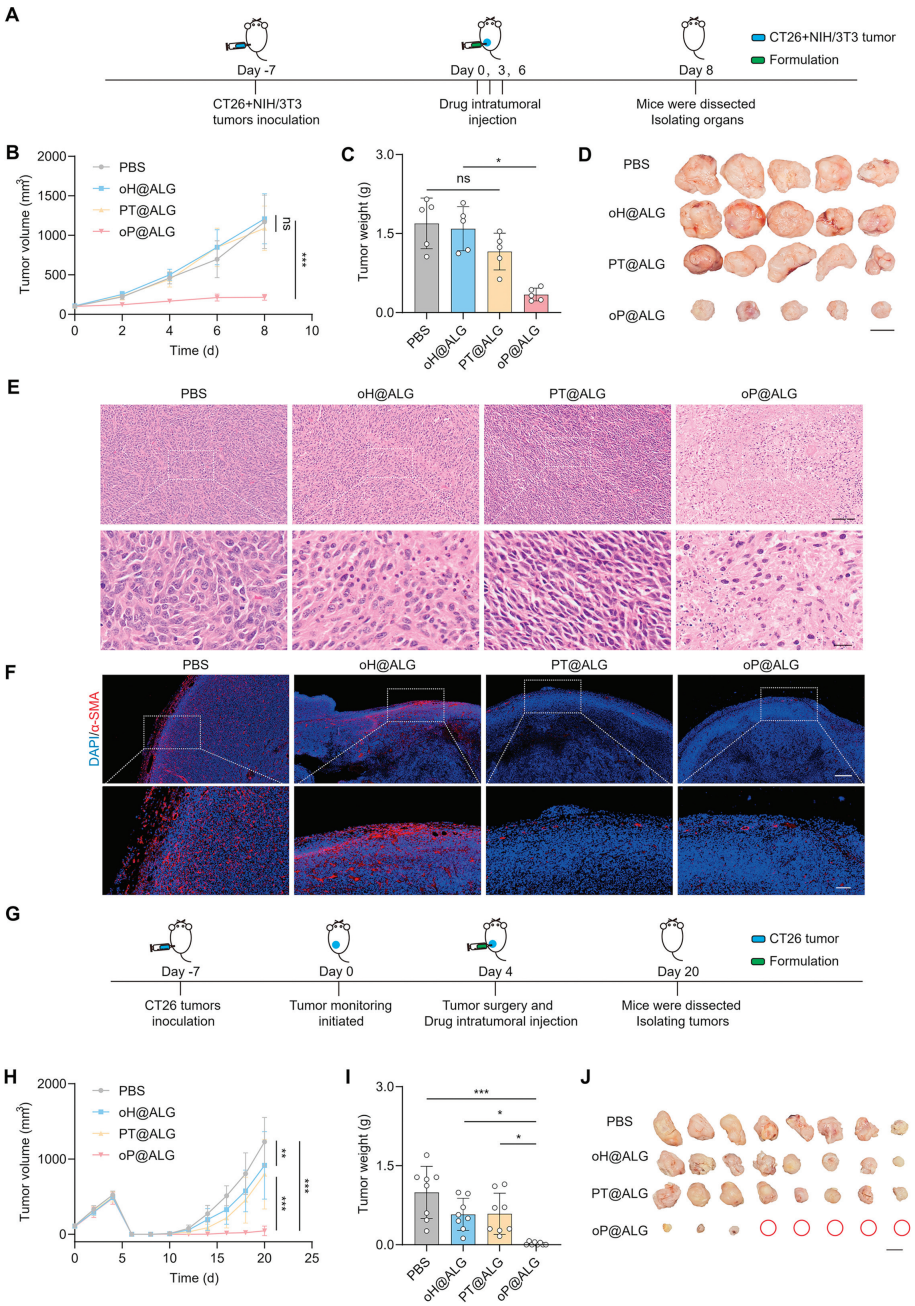

Fig. 5. oP@ALG exhibited significant antitumor efficacy in the stroma-rich subcutaneous tumor model and effectively suppressed tumor recurrence in the post-tumor resection model. (A) Schematic illustration of oH@ALG, PT@ALG and oP@ALG treatment in CT26 + NIH/3T3 subcutaneous tumor models. (B) The tumor growth profiles, (C) the tumor weight, and (D) tumor photos after various treatments. $n = 5$. Scale bar: 10 mm. (E) H&E staining of tumor tissue sections after various treatments at day 8. Scale bar: 100 μm (at low magnification), 20 μm (at high magnification). (F) Immunofluorescence staining of α-SMA of tumor tissue sections after various treatments at day 8. Scale bar: 400 μm (at low magnification), 100 μm (at high magnification). (G) Schematic illustration of the dosing regimens of oH@ALG, PT@ALG, and oP@ALG in the postoperative recurrence model of CT26 subcutaneous tumors. (H) The tumor growth profiles, (I) the tumor weight, and (J) tumor photos after various treatments. $n = 8$. Scale bar: 10 mm. Data are displayed as mean ± SD. Statistical significance was analyzed by one-way ANOVA with a Tukey *post hoc* test. $^{*}P < 0.05$, $^{**}P < 0.01$, $^{***}P < 0.001$.

site immediately after surgical removal of the tumor significantly reduced tumor recurrence and growth. A more in-depth examination of the reasons behind, the oP@ALG hydrogel system was injected at the surgical resection site to utilize the differential release of small molecule drugs and OVs by the hydrogel, and the fast-releasing PT-100 normalized the CAFs and reduced the incompletely resected tumor stroma, so that the slow-releasing oH2 infected and killed the residual tumor cells was further enhanced. These results demonstrate that the oP@ALG hydrogel system shows excellent therapeutic efficacy not only in the CT26 subcutaneous tumor model, but also in close-to-clinical tumor models, such as the stroma-rich subcutaneous tumor model and the post-tumor resection model, which show a strong ability to inhibit tumor growth. In the future, we will continue to validate the great application potential of oP@ALG in other tumor models.

In conclusion, we developed a stable, controllable, simple and easy-to-prepare functional hydrogel that employed a differential release strategy of hydrogel-loaded two drugs to enhance oncolytic HSV-mediated cancer immunotherapy. This hydrogel consisted of oH2 oncolytic herpesvirus particles encapsulated within ALG and the anti-CAF small molecule drug PT-100. Shedding of oH2 into non-target tissues was reduced by hydrogel loading. The

fast-releasing PT-100 acted as an anti-CAFs drug to normalize CAFs, reduced ECM and decreased interstitial pressure at the tumor site, and then the slow-releasing oH2 infected and killed tumor cells more effectively. The hydrogel strategy of differential release of the two drugs synergistically promoted immune cell infiltration and cytotoxicity, which built an anti-tumor immune microenvironment and improved the efficacy of OVs. It provides a promising paradigm for highly effective, low-toxicity OVs therapy and is particularly applicable to stroma-rich tumor types.

Declaration of competing interest

The authors declare that they have no known competing financial interests or personal relationships that could have appeared to influence the work reported in this paper.

CRediT authorship contribution statement

Xiaoyu Hou: Writing – original draft, Visualization, Investigation, Data curation. **Mingyang Liu:** Writing – original draft, Visualization, Investigation, Data curation. **Hu Wu:** Writing – original draft, Visualization, Investigation. **Nan Wang:** Investigation. **Xu Zhao:** Writing – review & editing, Data curation. **Xifeng Qin:** Data curation. **Xiaomin Su:** Data curation. **Hanwei Huang:** Writing – original draft. **Zihan Ma:** Data curation. **Jiahao Liu:** Visualization. **Onder Ergonul:** Writing – review & editing. **Füsun Can:** Writing – review & editing. **Wei Liu:** Writing – review & editing, Conceptualization. **Zhiqing Pang:** Supervision, Methodology, Conceptualization. **Funan Liu:** Supervision, Methodology, Conceptualization.

Acknowledgments

The authors thank the staff members of the Binhui Biopharmaceutical Co., Ltd. (Wuhan, China) for providing technical support and Shiyanjia Lab (www.shiyanjia.com) for providing invaluable assistance with the cryo-SEM analysis. This work was supported by the National Key R&D Program of China (No. 2022YFC2403401), the National Natural Science Foundation of China (Nos. 82073368, 82303766), the Liaoning Revitalization Talents Program (No. XLYC2007071), the China Postdoctoral Science Foundation (No. 2023M743908) and the Joint Program of Science and Technology Program of Liaoning Province (No. 2023JH2/101700094).

Supplementary materials

Supplementary material associated with this article can be found, in the online version, at doi:10.1016/j.cclet.2024.110106.

References

[1] S.Z. Shalhout, D.M. Miller, K.S. Emerick, H.L. Kaufman, Nat. Rev. Clin. Oncol. 20 (2023) 160–177.
[2] D.N. Lin, Y.N. Shen, T.B. Liang, Signal Transduct. Target. Ther. 8 (2023) 156.
[3] H.W. Huang, M.Y. Liu, M.C. Sun, et al., ACS Nano 17 (2023) 14461–14474.
[4] Q. Wu, H.W. Huang, M.C. Sun, et al., Adv. Mater. 35 (2023) e2212210.
[5] M.Y. Liu, R.Z. Zhang, H.W. Huang, et al., Adv. Sci. 11 (2024) e2303907.
[6] M. Fusciello, F. Fontana, S. Tähtinen, et al., Nat. Commun. 10 (2019) 5747.
[7] P.J. Wang, X.Z. Li, J.W. Wang, et al., Nat. Commun. 8 (2017) 1395.
[8] B. Xu, L. Tian, J. Chen, et al., Nat. Commun. 12 (2021) 5908.
[9] J. Martinez-Quintanilla, I. Seah, M. Chua, K. Shah, J. Clin. Invest. 129 (2019) 1407–1418.
[10] L.Q. Fu, X.B. Ma, Y.T. Liu, Z.G. Xu, Z.J. Sun, Chin. Chem. Lett. 33 (2022) 1718–1728.
[11] A. Ribas, R. Dummer, I. Puzanov, et al., Cell 170 (2017) 1109–1119 e10.
[12] B.D. Lichty, C.J. Breitbach, D.F. Stojdl, J.C. Bell, Nat. Rev. Cancer 14 (2014) 559–567.
[13] W.Y. Ban, J.H. Guan, H.W. Huang, et al., Nano Res. 15 (2022) 4137–4153.
[14] S.J. Russell, K.W. Peng, J.C. Bell, Nat. Biotechnol. 30 (2012) 658–670.
[15] B. Sangro, G. Mazzolini, J. Ruiz, et al., J. Clin. Oncol. 22 (2004) 1389–1397.
[16] R. Ma, Z.L. Li, E.A. Chiocca, M.A. Caligiuri, J.H. Yu, Trends Cancer 9 (2023) 122–139.
[17] Y. Chao, L.G. Xu, C. Liang, et al., Nat. Biomed. Eng. 2 (2018) 611–621.
[18] T. Funami, Y.P. Fang, S. Noda, et al., Food Hydrocolloids 23 (2009) 1746–1755.
[19] S.J. Yuan, W.W. Mu, S.J. Liu, et al., ACS Nano 17 (2023) 13611–13626.
[20] H. Soliman, D. Hogue, H. Han, et al., Nat. Med. 29 (2023) 450–457.
[21] C.M. Kelly, C.R. Antonescu, T. Bowler, et al., JAMA Oncol. 6 (2020) 402–408.
[22] J. Martín-Broto, D.S. Moura, B.A. Van Tine, Clin. Cancer Res. 26 (2020) 5801–5808.
[23] E. Ramelyte, A. Tastanova, Z. Balázs, et al., Cancer Cell 39 (2021) 394–406 e4.
[24] J.A. Chesney, A. Ribas, G.V. Long, et al., J. Clin. Oncol. 41 (2023) 528–540.
[25] B. Zhang, J. Huang, J.L. Tang, et al., J. Immunother. Cancer 9 (2021) e002224.
[26] X.M. Su, Y.B. Cao, Y. Liu, et al., Mater. Today Bio 12 (2021) 100154.
[27] Y.Y. Xu, S.Y. Zhao, Z.Z. Weng, et al., ACS Appl. Mater. Interfaces 12 (2020) 54497–54506.
[28] G.T. Liu, Y. Zhou, Z.J. Xu, et al., Chin. Chem. Lett. 34 (2023) 107705.
[29] Y.K. Li, H.Y. Zheng, Y.X. Liang, et al., Chin. Chem. Lett. 33 (2022) 5030–5034.
[30] F. Abasalizadeh, S.V. Moghaddam, E. Alizadeh, et al., J. Biol. Eng. 14 (2020) 8.
[31] S. Brulé, M. Levy, C. Wilhelm, et al., Adv. Mater. 23 (2011) 787–790.
[32] C.N. Zhang, G.N. Shi, J. Zhang, et al., J. Control. Release 256 (2017) 170–181.
[33] H.B. Hao, S.P. Wu, J.K. Lin, et al., Nat. Biomed. Eng. 7 (2023) 928–942.
[34] Y. Liu, B. Zhuang, B.C. Yuan, et al., Acta Pharm. Sin. B 13 (2023) 315–326.
[35] X. Duan, Y. Zhang, M.R. Guo, et al., Acta Pharm. Sin. B 13 (2023) 942–954.
[36] X.Q. Hao, X.W. Zhang, Y. Hu, et al., Chin. Chem. Lett. 34 (2023) 107965.
[37] K.C. Valkenburg, A.E. de Groot, K.J. Pienta, Nat. Rev. Clin. Oncol. 15 (2018) 366–381.
[38] X.M. Chen, E.W. Song, Nat. Rev. Drug Discov. 18 (2019) 99–115.
[39] X.Q. Mao, J. Xu, W. Wang, et al., Mol. Cancer 20 (2021) 131.
[40] H.Q. Liu, Y. Shi, F. Qian, Adv. Drug Deliv. Rev. 172 (2021) 37–51.
[41] J. Barbazan, C. Pérez-González, M. Gómez-González, et al., Nat. Commun. 14 (2023) 6966.
[42] A. Allam, M. Yakou, L. Pang, M. Ernst, J. Huynh, Front. Immunol. 12 (2021) 767939.
[43] Z. Wen, Q.F. Liu, J.H. Wu, et al., Ann. Transl. Med. 7 (2019) 532.
[44] Y.K. Huang, Y. Chen, S.L. Zhou, et al., Nat. Commun. 11 (2020) 622.
[45] X.X. Han, Y.Y. Li, Y. Xu, et al., Nat. Commun. 9 (2018) 3390.